NUMERICAL STUDY OF DEVELOPING LAMINAR MIXED CONVECTION IN A HEATED ANNULAR DUCT WITH TEMPERATURE DEPENDENT PROPERTIES

by

Meriem KHEMICI, Toufik BOUFENDI *, and Sofiane TOUAHRI

Laboratory of Energy Physics, Department of Physics, Faculty of Exact Science,
University Freres Mentouri Constantine 1, Constantine, Algerie

Original scientific paper
https://doi.org/10.2298/TSCI171013079K

This study presents a numerical simulation of the 3-D laminar mixed convection between two concentric horizontal cylinders with physical properties which depend on temperature. The outer cylinder is subjected to an internal energy generated by the Joule effect whereas the inner cylinder is adiabatic. The flow and thermal fields are modeled by the continuity, momentum, and energy equations with appropriate initial and boundary conditions using a cylindrical co-ordinate system. The model equations are numerically solved by a finite volume method with a second order accurate spatiotemporal discretization. For the considered geometric, dynamic and thermal controlling parameters, it is found that the transverse flow is always the cause of the circumferential variation of the temperature and the physical properties of the fluid. The phenomenon of the temperature stratification is highlighted and the vortices obtained lead to an improvement in the heat transfer quantified by the increase in the number of Nusselt. The obtained axial Nusselt number increases with the increased of Grashof number which is proportional to the heat flux imposed at the surface of the outer cylinder.

Key words: *mixed convection, concentric cylinders, temperature dependent properties, finite volume method*

Introduction

Mixed convection heat transfer in a horizontal annulus between concentric cylinders has attracted considerable amount of numerical and experimental works because of its technical importance, as it is present in numerous engineering applications such as gas-cooled electrical cables, and double-pipe heat exchangers, just to mention a few examples. Several kinds of convective flows which are dependent on geometric, dynamic and thermal controlling parameters such as the aspect ratio, the Prandtl, Reynolds, and Grashof numbers can be developed. Rao *et al.* [1] investigated the flow patterns of air (Pr = 0.7) and found three flow regimes depending on diameter ratio (D_i/L): a 2-D oscillatory flow for $D_i/L < 2.8$, a 3-D spiral flow for: $2.8 < D_i/L < 8.5$ and a 2-D multicellular flow for $D_i/L > 8.5$. Ouazzane *et al.* [2] presented a numerical and experimental approach to the problem of mixed convection between two horizontal plans at different temperatures. The results of this numerical study show a movement in the form of transverse rolls moving in the direction of flow movement. The experimental results obtained with air show a structure of the flow in the form of transverse rolls for the low values

* Corresponding author, e-mail: tboufendi@umc.edu.dz

of the Reynolds number and longitudinal vortices for higher numbers of Reynolds number. A linear stability analysis of the fully developed flow is performed by Chenier *et al.* [3] for air flowing in an annular pipe of fixed radius ratio equal to 1.2. The synthesis of the results on the transitions permits to build the map of stability for the steady and established mixed convection flows. A stability diagram in the (Pe,Ra)-plane was drawn to define the stability regions of the secondary flows. Hu *et al.* [4] studied the multiple steady solutions in natural convection between horizontal concentric cylinders with a constant heat flux wall, a fixed aspect ratio equals to 2 is considered. It was found a new steady solution consisting more of eddies when the Rayleigh number exceeds a certain critical value. Mojtabi and Caltagirone [5] studied numerically the laminar mixed convection hydrodynamically and thermally developed between two horizontal coaxial cylinders. It was found that the exchange of heat at the two cylinders depends only on the Rayleigh and Prandtl numbers and the radii ratio. Forced and free convective heat transfer for thermally developing and thermally fully developed laminar air-flow inside horizontal concentric annuli has been experimentally investigated by Mohammed *et al.* [6]. The result was that the axial Nusselt number increases with the Reynolds number. Kotake and Hattori [7] studied numerically a combined forced and free convection flows in a horizontal annulus with the finite-difference method. The fluid in an annulus is heated axially with uniform heat flux at the walls. With the numerical results, the flow features of combined forced and free convection in the annulus are studied. The vortex associated increases its strength with the Grashof number, especially more rapidly in the case of inner wall heating. Nazrul *et al*. [8] studied numerically the laminar mixed convection heat transfer in a horizontal annulus. The fluids used are air and water. The thermal boundary conditions are: uniform heat flux at the inner wall and an adiabatic outer wall. The results obtained show that the secondary flow is more intense in the upper part of the cross-section. The Nusselt number at the end of the entrance zone is about 30% higher than that of pure forced convection for a ratio of radius of 1.5 and 110% higher than that of forced convection for a ratio of radius of 10. The effect of variable fluid properties on the mixed convection has been numerically studied by Touahri and Boufendi. [9, 10] with a 3-D conjugate heat transfer in an annular space between two horizontal cylinders, the external cylinder heated by an electric current passing through its small thickness and the internal cylinder being insulated. The thermal convection in the fluid domain is conjugated to the thermal conduction in the solid. The results obtained show the 3-D aspect of the thermal and dynamics fields with considerable variation of the viscosity and moderate variation of the fluid thermal conductivity. The mixed convection Nusselt number becomes more superior to that of forced convection when the Grashof number is increased. Recently, the (2-D) fully developed mixed convection equations in vertical annulus are analytically resolved for obtain exact solutions in terms of Bessel's functions and modified Bessel's functions of first and second kinds, by Basant *et al.*[11] and Oni [12] for different purposes. The first [11] exploit these solutions to study the influence of both heat generating and absorbing fluid by considering one micro-concentric-annulus while in [12] the authors treat the effects of different parameters such as heat source, thermal radiation and porosity on mixed convection flow, considering the case of an annular space filled with a porous material. At this stage of research development on the improvement of convective heat transfer in annular geometry, special interest has been given to nanofluid flows [13] and fluid properties thermal dependence [14].

In this work, we have studied numerically the heat transfer by mixed convection in an annular space between two concentric cylinders, the physical properties of the fluid are thermally dependent and heat losses with the external environment are considered. The aim of this

work is to study the variations of the thermal and dynamic fields as a function of the volumetric heating and the effects of the increase of this heating on the Nusselt number and heat transfer.

Mathematical model

The geometry of the studied system is illustrated in fig.1. We consider two horizontal concentric cylinders having a length L = 1 m. The inner cylinder has the inside diameter $D_{1i} = 0.56$ cm and the outside diameter $D_{1o} = 0.60$ cm, the external cylinder has the inside diameter $D_{2i} = 0.96$ cm and the outside diameter $D_{2o} = 1$ cm. The cylinders are made of Inconel having a thermal conductivity K_s = 20 W/mK. The passing of an electrical intensity along the thickness of external cylinder produced a generation of heat by the Joule effect. This heat is transferred to laminar incompressible flow of distilled water (Pr = 8.082), while the inner cylinder is considered perfectly insulated (adiabatic). The thermo-dependence effect of the physical properties $\mu^*(T^*)$ and $K^*(T^*)$ on the heat transfer is considered and their variation with temperature was determined by Baehr and Stephan [15]. The flow at the entrance system is of Poiseuille type, with a Re = 373.28 and a constant temperature equal at 15 °C.

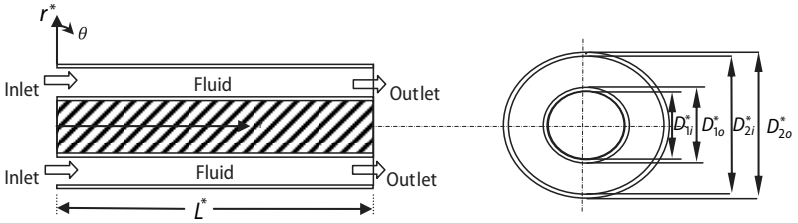

Figure 1. Geometry of the problem

Mixed convection flow in the annulus formed by two concentric horizontal cylinders is modeled by the mass conservation, momentum and energy equations using the initial and boundary conditions, and written in cylindrical co-ordinates which are better suited to the geometry studied.

– At $t^* = 0$:

$$V_r^* = V_\theta^* = V_z^* = T^* = 0 \tag{1}$$

– At $t^* > 0$ mass conservation equation:

$$\frac{1}{r^*}\frac{\partial}{\partial r^*}\left(r^* V_r^*\right) + \frac{1}{r^*}\frac{\partial V_\theta^*}{\partial \theta} + \frac{\partial V_z^*}{\partial z^*} = 0 \tag{2}$$

– Radial momentum conservation equation:

$$\frac{\partial V_r^*}{\partial t^*} + \frac{1}{r^*}\frac{\partial}{\partial r^*}\left(r^* V_r^* V_r^*\right) + \frac{1}{r^*}\frac{\partial}{\partial \theta}\left(V_\theta^* V_r^*\right) + \frac{\partial}{\partial z^*}\left(V_z^* V_r^*\right) - \frac{V_\theta^{*2}}{r^*} =$$
$$= -\frac{\partial P^*}{\partial r^*} + \frac{Gr_0^*}{\mathrm{Re}_0^2}\cos\theta T^* + \frac{1}{\mathrm{Re}_0}\left[\frac{1}{r^*}\frac{\partial}{\partial r^*}\left(r^* \tau_{rr}^*\right) + \frac{1}{r^*}\frac{\partial}{\partial \theta}\left(\tau_{r\theta}^*\right) - \frac{\tau_{\theta\theta}^*}{r^*} + \frac{\partial}{\partial z^*}\left(\tau_{rz}^*\right)\right] \tag{3}$$

– Angular momentum conservation equation:

$$\frac{\partial V_\theta^*}{\partial t^*}+\frac{1}{r^*}\frac{\partial}{\partial r^*}\left(r^* V_r^* V_\theta^*\right)+\frac{1}{r^*}\frac{\partial}{\partial \theta}\left(V_\theta^* V_\theta^*\right)+\frac{\partial}{\partial z^*}\left(V_z^* V_\theta^*\right)+\frac{V_r^* V_\theta^*}{r^*}=$$
$$=-\frac{1}{r^*}\frac{\partial P^*}{\partial \theta}-\frac{\mathrm{Gr}_0^*}{\mathrm{Re}_0^2}\sin\theta T^*+\frac{1}{\mathrm{Re}_0}\left[\frac{1}{r^{*2}}\frac{\partial}{\partial r^*}\left(r^{*2}\tau_{\theta r}^*\right)+\frac{1}{r^*}\frac{\partial}{\partial \theta}\left(\tau_{\theta\theta}^*\right)+\frac{\partial}{\partial z^*}\left(\tau_{\theta z}^*\right)\right] \tag{4}$$

– Axial momentum conservation equation:

$$\frac{\partial V_z^*}{\partial t^*}+\frac{1}{r^*}\frac{\partial}{\partial r^*}\left(r^* V_r^* V_z^*\right)+\frac{1}{r^*}\frac{\partial}{\partial \theta}\left(V_\theta^* V_z^*\right)+\frac{\partial}{\partial z^*}\left(V_z^* V_z^*\right)=$$
$$=-\frac{\partial P^*}{\partial z^*}+\frac{1}{\mathrm{Re}_0}\left[\frac{1}{r^*}\frac{\partial}{\partial r^*}\left(r^*\tau_{rz}^*\right)+\frac{1}{r^*}\frac{\partial}{\partial \theta}\left(\tau_{\theta z}^*\right)+\frac{\partial}{\partial z^*}\left(\tau_{zz}^*\right)\right] \tag{5}$$

– Energy conservation equation:

$$\frac{\partial T^*}{\partial t^*}+\frac{1}{r^*}\frac{\partial}{\partial r^*}\left(r^* V_r^* T^*\right)+\frac{1}{r^*}\frac{\partial}{\partial \theta}\left(V_\theta^* T^*\right)+\frac{\partial}{\partial z^*}\left(V_z^* T^*\right)=$$
$$=G^*-\frac{1}{\mathrm{Re}_0\,\mathrm{Pr}_0}\left[\frac{1}{r^*}\frac{\partial}{\partial r^*}\left(r^* q_r^*\right)+\frac{1}{r^*}\frac{\partial}{\partial \theta}\left(q_\theta^*\right)+\frac{\partial}{\partial z^*}\left(q_z^*\right)\right] \tag{6}$$

where

$$G^*=\begin{cases}\dfrac{K_S^*}{\mathrm{Re}_0\,\mathrm{Pr}_0} & \text{in the solid}\\ 0 & \text{in the fluid}\end{cases}$$

The viscous stress tensor components are:

$$\tau_{rr}^*=2\mu^*\frac{\partial V_r^*}{\partial r^*}\quad \tau_{\theta\theta}^*=2\mu^*\left[\frac{1}{r^*}\frac{\partial V_\theta^*}{\partial \theta}+\frac{V_r^*}{r^*}\right]\quad \tau_{r\theta}^*=\tau_{\theta r}^*=\mu^*\left[r^*\frac{\partial}{\partial r^*}\left(\frac{V_\theta^*}{r^*}\right)+\frac{1}{r^*}\frac{\partial V_r^*}{\partial \theta}\right]$$
$$\tau_{zz}^*=2\mu^*\frac{\partial V_z^*}{\partial z^*}\quad \tau_{zr}^*=\tau_{rz}^*=\mu^*\left[\frac{\partial V_z^*}{\partial r^*}+\frac{\partial V_r^*}{\partial z^*}\right]\quad \tau_{\theta z}^*=\tau_{z\theta}^*=\mu^*\left[\frac{\partial V_\theta^*}{\partial z^*}+\frac{1}{r^*}\frac{\partial V_z^*}{\partial \theta}\right] \tag{7}$$

The heat fluxes are:

$$q_r^*=-K^*\frac{\partial T^*}{\partial r^*},\quad q_\theta^*=-\frac{K^*}{r^*}\frac{\partial T^*}{\partial \theta^*}\quad \text{and}\quad q_z^*=-K^*\frac{\partial T^*}{\partial z^*} \tag{8}$$

Boundary conditions

– At the annulus entrance: $z^*=0$
  – In the fluid domain: $0.83\le r^*\le 1.33$ and $0\le\theta\le 2\pi$

$$V_r^*=V_\theta^*=T^*=0,\quad V_z^*=1 \tag{9}$$

  – In the solid domain: $0.77\le r^*\le 0.83$ or $1.33\le r^*\le 1.38$ and $0\le\theta\le 2\pi$

$$V_r^*=V_\theta^*=V_z^*=T^*=0 \tag{10}$$

– At the annulus exit: $z^* = 277.77$
  – In the fluid domain: $0.83 \le r^* \le 1.33$ and $0 \le \theta \le 2\pi$

$$\frac{\partial V_r^*}{\partial z^*} = \frac{\partial V_\theta^*}{\partial z^*} = \frac{\partial V_z^*}{\partial z^*} = \frac{\partial}{\partial z^*}\left(K^* \frac{\partial T^*}{\partial z^*} \right) = 0 \tag{11}$$

  – In the solid domain: $0.77 \le r^* \le 0.83$ or $1.33 \le r^* \le 1.38$ and $0 \le \theta \le 2\pi$

$$V_r^* = V_\theta^* = V_z^* = \frac{\partial}{\partial z^*}\left(K^* \frac{\partial T^*}{\partial z^*} \right) = 0 \tag{12}$$

– At the inside wall of internal pipe: $r^* = 0.77$

$$V_r^* = V_\theta^* = V_z^* = 0 \quad \text{and} \quad \frac{\partial T^*}{\partial r^*} = 0 \tag{13}$$

– At the outer wall of external pipe: $r^* = 1.38$

The conductive heat flux is equal to the sum of the heat fluxes of the radiation and natural convection losses.

– for $0 \le \theta \le 2\pi$ and $0 \le z^* \le 277.77$

$$\begin{cases} V_r^* = V_\theta^* = V_z^* = 0 \\ -K^* \dfrac{\partial T^*}{\partial r^*} = \dfrac{\left(h_r + h_c\right) D_i}{K_0} T^* \end{cases} \tag{14}$$

where

$$h_r = \varepsilon\sigma(T^2 + T_\infty^2)(T + T_\infty) \tag{15}$$

The emissivity of the outer wall ε is arbitrarily chosen to 0.9 while h_c is derived from the correlation of Churchill and Chu [16] valid for all Prandtl number and for Rayleigh numbers in the range $10^{-6} \le \mathrm{Ra} \le 10^9$.

$$\mathrm{Nu} = \frac{h_c D_i}{K_{\mathrm{air}}} = \left\{ 0.6 + \frac{0.387\,\mathrm{Ra}^{1/6}}{\left[1 + \left(\dfrac{0.559}{\mathrm{Pr}_{\mathrm{air}}} \right)^{9/16} \right]^{8/27}} \right\}^2 \tag{16}$$

The Rayleigh and the Prandtl numbers defined, respectively, as:

$$\mathrm{Ra} = \frac{\mathrm{g}\beta\left[T\left(R_o, \theta, z\right) - T_\infty \right] D_o^3}{\alpha_{\mathrm{air}} \nu_{\mathrm{air}}}, \quad \mathrm{Pr}_{\mathrm{air}} = \frac{\nu_{\mathrm{air}}}{\alpha_{\mathrm{air}}} \tag{17}$$

Nusselt numbers

At the solid-fluid interface, the local Nusselt number $\mathrm{Nu}(\theta, z^*)$ is defined:

$$\mathrm{Nu}(\theta, z^*) = \frac{h(\theta, z^*) D_i}{K_0} = \left[\frac{K^* \left. \dfrac{\partial T^*}{\partial r^*} \right|_{r^*=1.33}}{T^*(1.33, \theta, z^*) - T_b^*(z^*)} \right] \tag{18}$$

where the dimensionless bulk fluid temperature is given by:

$$T_b^*\left(z^*\right) = \frac{\int_{0.83}^{1.33} \int_0^{2\pi} V^*\left(r^*, \theta, z^*\right) T^*\left(r^*, \theta, z^*\right) r^* \mathrm{d}r^* \mathrm{d}\theta}{\int_{0.83}^{1.33} \int_0^{2\pi} V^*\left(r^*, \theta, z^*\right) r^* \mathrm{d}r^* \mathrm{d}\theta}$$

The axial Nusselt number is defined:

$$\mathrm{Nu}(z^*) = \frac{1}{2\pi} \int_0^{2\pi} \mathrm{Nu}(\theta, z^*) \mathrm{d}\theta \tag{19}$$

Numerical method

The finite volume method, well exposed by Patankar [17], is applied to discretize the physical domain and the model equations with boundary conditions. The numerical grid used is uniform along each cylindrical co-ordinate direction. The mesh-independent study has been realized with three different grids: 26×34×142, 26×44×162, and 52×88×162 in the radial, azimutal and axial directions respectively. For a proper choice of the appropriate mesh, several executions of the calculation code have been made. We find that the last two mesh give results, qualitatively and quantitatively, quasi-similar. As, for example, the absolute difference between the values of the average Nusselt numbers does not exceed 5%. Then, we preferred to choose the 26×44×162 mesh, to gain in computing time. A graphical representation of the used numerical grid is shown in fig. 2.

The discretization of the equations is based on the calculation of the integrals of the partial differential equations terms by terms on each control volume to obtain the discretized algebraic equations. The spatiotemporal numerical discretization is second order accurate: the numerical errors are of order $(\Delta r^*)^2$, $(\Delta z^*)^2$, $(\Delta\theta)^2$ and $(\Delta t^*)^2$. The considered time step is $\Delta t^* = 5 \cdot 10^{-4}$. In fig. 3 we illustrate axial evolution of the circumferentially mean local axial Nusselt number It is seen that there is good agreement between our results and those of Carlo and Guidice [18] who studied numerically the conjugate mixed convection heat transfer in annulus with the controlling parameters of the problem: Re = 1000, Pr = 0.7, Gr = 10^6, and $R_2/R_1 = 1$

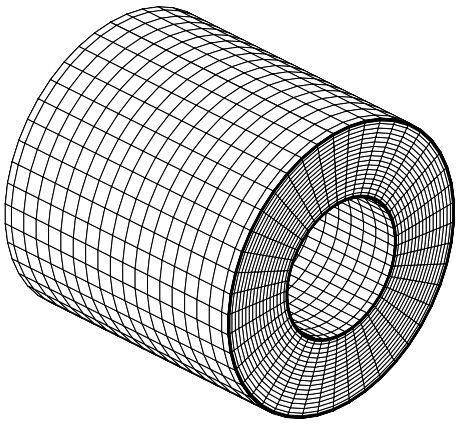

Figure 2. Numerical grid used

Results and discussions

The discussion presented here is pertinent to the study of the 3-D laminar mixed convection heat

transfer in an annular space. The studied Grashof numbers are: 1432.55, 1813.07, 2238.35, 2708.41, 3223.23 and 3781.98, the Reynolds number fixed at 373.28 and the Prandtl number equal to 8.082. In the following discussions, we present results that include details of the flow and temperature fields in addition to axial Nusselt numbers for different Grashof numbers. The obtained flow for the studied cases is characterized by a main flow along the axial direction and a secondary flow influenced by the density variation with temperature.

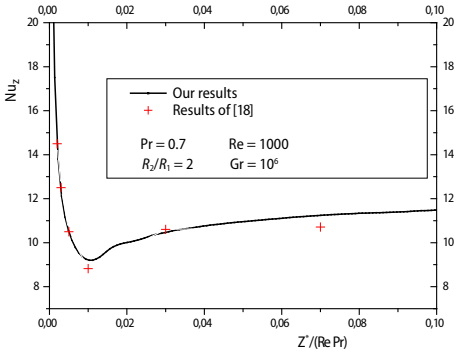

Figure 3. Axial evolution of the circumferentially mean local axial Nusselt number; a comparison with the results of Carlo and Guidice [18]

The transverse fluid motion and velocity field

The numerical solution of the hydrodynamically and thermally developing mixed convection with temperature dependent physical properties is obtained by solving eqs. (2)-(6) with the conditions specified by eqs. (9)-(17). The Grashof number is varied. The results revealed that the flow is hydrodynamically and thermally developing from the annulus inlet to the annulus exit. The flow field is composed of the main axial flow (represented by the axial component of the velocity V_z^*) and a secondary flow (represented by the radial and angular components of the velocity). The secondary flow, in a given conduit cross section, may also be conveniently represented by the contours of the 2-D stream functions of the radial and angular components of the velocity. Close to the entrance of the system, the temperature is constant and the secondary flow is inexistent. Away from the annular space entrance, a secondary flow is present; the secondary flow is induced by the buoyancy forces and intensifies gradually in the axial direction and its momentum increases with the Grashof number. The form of the buoyancy induced secondary flow depends on the Grashof number. The secondary flow for Gr = 3781.98 is illustrated in fig. 4 at selected axial positions z^* =13.02, 68.58, 174.479, L^*, where 174.479 is the axial position where the secondary flow is more intense. In the domain $33.85 < z^* < L^*$, this flow is accompanied by two identical counter-rotating cells in the plan ($r^* - \theta$) that each vortex circulates in one half section at the opposed direction. This flow is well explained by the buoyancy effect since the flow rises along the wall of the heated outer cylinder (presented in fig. 4 by the red color) and descends along the relatively colder adiabatic wall of the inner cylinder (presented in fig. 4 by the blue color). In tab. 1, we present the radial, axial and angular position of $V_{\theta\max}^*$ for different studied Grashof numbers.

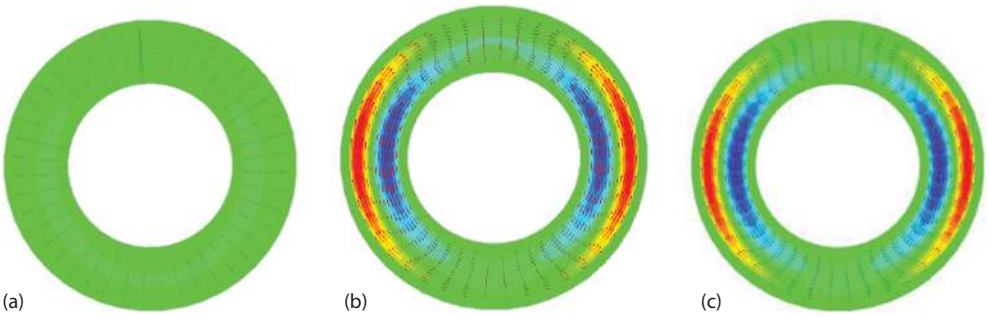

Figure 4. Secondary flow for Gr = 3781.98 at given positions: (a) z^* = 13.021, (b) z^* = 174.479, and (c) z^* = 277.77 (*for color image see journal web site*)

Table 1. Positions of the maximum velocity $V^*_{\theta\,\max}$ for different Grashof numbers

Gr	$V^*_{\theta\,\max}$	r^*	z^*	θ
1432.55	0.0103	1.2239	277.77	4.7837
1813.07	0.0124	1.2239	277.77	4.7837
2238.35	0.0144	1.2239	277.77	4.7837
2708.41	0.0162	1.2239	277.77	4.7837
3223.23	0.0182	1.2239	188.37	4.7837
3781.98	0.0202	1.2239	174.48	4.7837

The effect of the buoyancy induced secondary flow on the axial flow is fairly well understood. Axisymmetric distribution of the axial flow is influenced by the generation of a transverse movement and by the variation of the viscosity as a function of the temperature, which causes an angular variation of the axial velocity, explained as follows: as the thermal viscosity is inversely proportional to the fluid temperature and the axial velocity increases with the decrease in the viscosity, a relatively high axial velocity will automatically be obtained in the upper part of the annular space where the temperature of the fluid is greater than that of the lower part. As seen in fig. 5 representing the variation of the axial velocity in the vertical plan which passes through the angles $\theta=0$ and $\theta=\pi$ which is a plan of symmetry for the following seven studied cases: Gr = 0 and Gr = 1432.55, 1813.07, 2238.35, 2708.41, 3223.23, and 3781.98. The results obtained clearly show that the effect of the decrease of the viscosity in the upper part of the annular space on the axial flow becomes more important with the increase of the volumetric heating, and that the effect of buoyancy force on the axial velocity becomes increasingly important with the increasing of heating volume. In tab. 2, we present the axial, radial and angular position of $V^*_{z\max}$ for different studied Grashof numbers.

On the other hand, fig. 6 shows the axial velocity profile $V^*_z(r^*)$ for different value of the angle, θ, at selected axial position $z^*=190.104$ and $z^*=277.777$ (at the annulus exit) for Grashof number equal to 3781.98, where $z^*=190.104$ is the axial position where the axial ve-

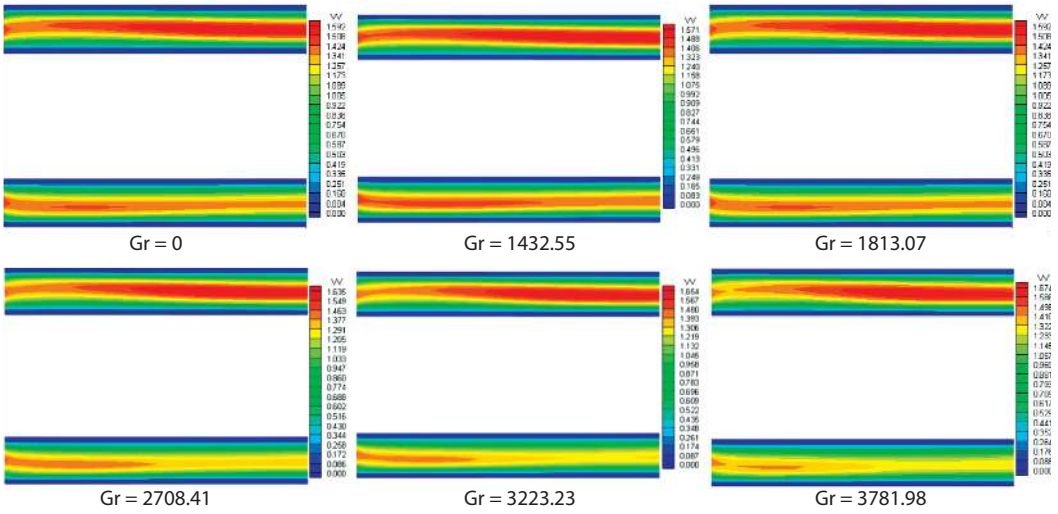

Figure 5. Development of axial flow in the vertical plane as a function of the Grashof number (*for color image see journal web site*)

Table 2. Maximum velocity positions $V^*_{z\,max}$ for different Grashof numbers

Gr	$V^*_{z\,max}$	z^*	r^*	θ
1432.55	1.571	230.035	1.067	0
1813.07	1.592	219.618	1.067	0
2238.35	1.613	214.409	1.067	0
2708.41	1.635	207.465	1.067	0
3223.23	1.654	197.049	1.067	0
3781.98	1.674	190.104	1.067	0

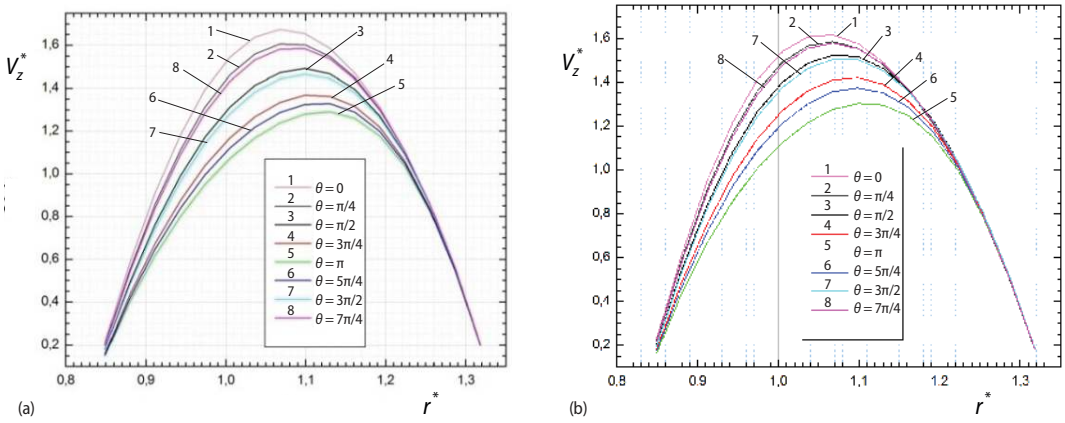

Figure 6. Axial velocity V_z^* profile for different values of the angle, θ, at (a) $z^* = 190.104$ and (b) $z^* = 277.7$ for Gr = 3781.98

locity is maximum, we note that the axial velocity is much greater near the outer cylinder in the upper half of the annular space where the temperature of the fluid is greater than that of the lower part. This fact is all the more markable when Grashof number is large. The axial velocity takes a minimum value at the pipes wall and a maximum value in the top part of the annulus, exactly at $z^* = 190.104$ and $\theta = 0$ which equal 1.674.

Temperature field and heat transfer

The fluid temperature is uniform at the annulus inlet. After, the flow is continuously heated in the axial direction leading to axial continue increase of the cross-section mixing average temperature. The internal energy generation induced by the Joule effect in outer cylinder creates a radial thermal gradient oriented towards the internal fluid such that the hot fluid is close to the wall of the external cylinder and the relatively cooler fluid is close to the wall of the internal cylinder. This fluid movement leads to a new temperature distribution for each axial section.The cross-section temperature at the annulus exit is illustrated in fig. 7 for the considered Grashof numbers equals 3781.98, 1432.55, and Gr = 0. The comparison of the temperature distribution clearly shows a wide qualitative and quantitative variation between forced and mixed convection. In the mixed convection flow the thermal field is considered symmetrical with respect to the vertical plane passing through $\theta = 0$ and $\theta = \pi$ but the comparison of the temperature distribution clearly shows a wide qualitative and quantitative variation between forced and mixed convection. In the mixed convection flow the thermal field is considered

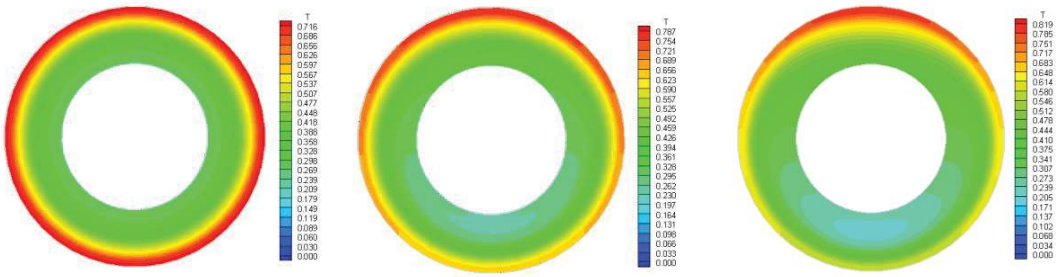

Figure 7. Isotherms distribution at the annulus exit $z^* = 277.77$ for the considered Grashof numbers (*for color image see journal web site*)

symmetrical with respect to the vertical plane passing through $\theta=0$ and $\theta=\pi$ but asymmetric with respect to the axis of the annulus. This is due to the mixing in a rotary direction caused by the secondary flow in the plane $(r^* - \theta)$. This movement of the secondary flow is the cause of the azimuthally temperature variation. However, due to the heat flow imposed on the wall, the maximum temperature must be at the inner wall of the outer cylinder in the plane of symmetry $\theta=0$.The thermal stratification at the upper part of the annular space is stable. Radially, the temperature decreases from the wall of the outer cylinder towards the wall of the inner cylinder, the minimum temperature is within the core fluid, in the lower part of the annulus at $\theta = \pi$. The mixed convection annulus maximum dimensionless temperature is equal to 0.787, 0.812, and 0.819 for Grashof numbers of 1432.55, 2708.41, and 3781.98, respectively. These values are higher than the forced convection annulus maximum dimensionless temperature equal to 0.716.

In fig. 8 an illustration will show the variation of temperature profile at the annulus exit $z^* = 277.77$ for different values of the Grashof numbers at the inner wall of the outer cylinder $r^* = 1.33$ and at outer wall of the inner cylinder $r^* = 0.83$, we note that the temperature is much greater in the upper half of the annular space than that of the lower part. To understand the effect of the buoyancy induced flow (secondary flow) on heat transfer, this may be accomplished by comparing the variations of the axial Nusselt numbers $\mathrm{Nu}(z^*)$. In fig. 9, it is seen that

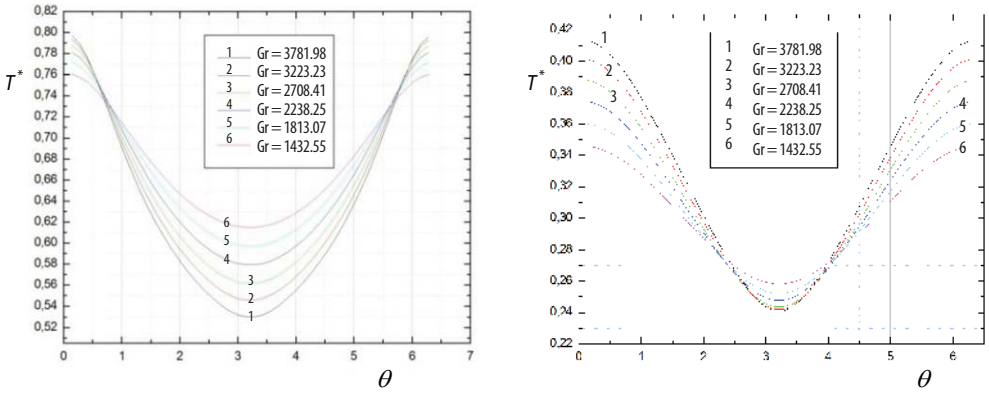

Figure 8. Variation of temperature profile at the annulus exit for different Grashof numbers at (a) $r^* = 0.83$ and (b) $r^* = 1.33$

from the entrance to $z^* = 43$, the large decrease of the axial Nusselt number is the same for all cases. This is comprehensible because in this zone, the buoyancy induced flow is very weak. From this zone to the exit, this secondary flow intensified rapidly and is enhanced by an increase of the Grashof number. The axial Nusselt number take a maximum value at the exit of the annulus equals to 5.847, 6.320, 6.566, 6.862, 7.208, 7.593, and 8.014 for Gr = 0, 1432.55, 1813.07, 2238.35, 2708.41, 3223.23, and 3781.98, respectively.

Figure 10 shows the angular variation of the local Nusselt number for a Gr = = 3781.98. From the entrance to the exit, we notice large axial and angular variations of local Nusselt numbers. For each given section, the local Nusselt number takes a minimum value at $\theta = 0$ and a maximum value at $\theta = \pi$.

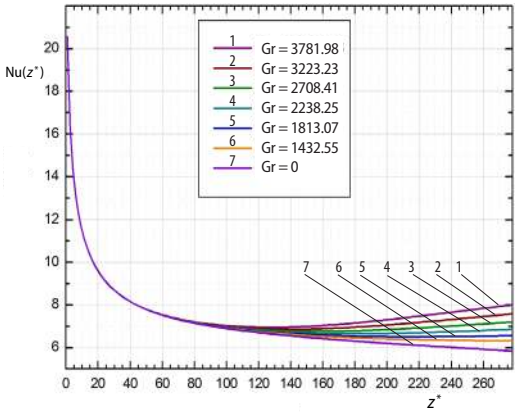

Figure 9. Axial Nusselt number variation at different Grashof numbers

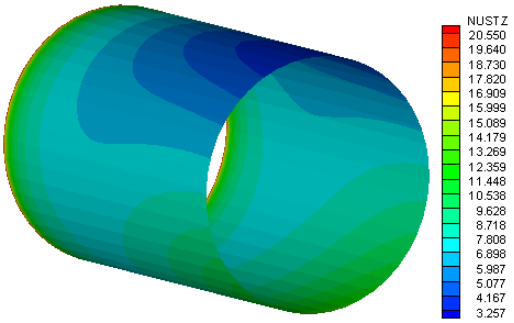

Figure 10. Local Nusselt number variation for Gr = 3781.98 (*for color image see journal web site*)

Conclusion

The numerical simulation of the mixed convection heat transfer between two horizontal pipes is studied. The external cylinder is heated by an electric current while the internal cylinder is insulated. The flow and thermal fields of the mixed convection with variable physical properties were presented. The results obtained show that the transverse flow is always the cause of the circumferential variation of the temperature and the physical properties of the fluid. While, the azimuthally variation of temperature in the given section is important; this phenomenon is demonstrated by the circumferential temperature variation of the wall. There is a large temperature wall difference between the top and bottom of the external cylinder. Although, the physical properties are thermally dependent (the dimensionless dynamic viscosity, μ^*, varies from 1.018 at the entrance to 0.232 at the exit) and finally, the obtained Nusselt number increases with the increase of volumetric heating.

Nomenclature

D – diameter, [m]
D_h – hydraulic diameter, $(= D_{2i} - D_{1o})$, [m]
G – volumetric heat generation, [$\mathrm{Wm^{-3}}$]
Gr^* – modified Grashof number, $(= g\beta G D_h^5 / K_s \nu^2)$, [–]
$h(\theta, z^*)$ – local heat transfer coefficient, [$\mathrm{Wm^{-2}K^{-1}}$]
h_c, h_r – convective, radiative local heat transfer coefficients respectively, [$\mathrm{Wm^{-2}K^{-1}}$]
K – fluid thermal conductivity, [$\mathrm{Wm^{-1}K^{-1}}$]
K^* – non-dimensional thermal conductivity, $(= K/K_0)$, [–]
L^* – non-dimensional annulus length $(= L/D_h)$, [–]
$\mathrm{Nu}(z^*)$ – axial Nusselt number $(= h(z)D_h/K_0)$, [–]
$\mathrm{Nu}(\theta, z^*)$ – local Nusselt number $(= h(\theta, z)D_h/K_0)$, [–]
P – pressure, [$\mathrm{Nm^{-2}}$]
P^* – non-dimensional pressure $[= (P - P_0)/\rho_0 V_0^2]$, [–]
Pr – Prandtl number $(= \nu/\alpha)$, [–]

q – heat flux, [Wm^{-2}]
r^* – non-dimensional radial co-ordinate (= r/D_h), [–]
Re – Reynolds number (= $V_0 D_h/\nu_0$), [–]
T – temperature, [K]
t – time, [s]
T^* – non-dimensional mixing cup temperature, [= $(T - T_0)/(GD_h^2/K_s)$], [–]
t^* – non-dimensional time (= $V_0 t/D_h$), [–]
V_r^*, V_θ^*, V_z^* – non-dimensional velocities components, (= $V_r/V_0, V_\theta/V_0, V_z/V_0$), [–]
V_0 – mean axial velocity at the annulus entrance, [ms^{-1}]
V_r, V_θ, V_z – radial, circumferential and axial velocities components, respectively, [ms^{-1}]
z^* – non-dimensional axial co-ordinate, (= z/D_h), [–]
z – axial co-ordinate

Greek symbols

α – thermal diffusivity, [m^{2}s^{-1}]
β – thermal expansion coefficient, [K^{-1}]
ε – emissivity coefficient , [–]
θ – angular co-ordinate, [rad]
μ – dynamic viscosity, [kgm^{-1}s^{-1}]
ν – kinematic viscosity, [m^{2}s^{-1}]
ρ – density, [kgm^{-3}]
σ – Stephan-Boltzmann constant (= 5.67·10^{-8}), [Wm^{-2}K^{-4}]

References

[1] Rao, Y-F., *et al.*, Flow Patterns of Natural Convection in Horizontal Cylindrical Annuli, *International Journal of Heat and Mass Transfer, 28* (1985), 3, pp. 705-714
[2] Ouazzani, M. T., *et al.*, Numerical and Experimental Study of Mixed Convection between Two Horizontal Plates at Different Temperatures, *International Journal of Heat and Mass Transfer, 32* (1989), 2, pp. 261-269
[3] Chenier, E., *et al.*, From Natural to Mixed Convection in Horizontal and Differentially Heated Annular Ducts: Linear Stability Analysis*, International Journal of Heat and Mass Transfer, 54* (2011), 23-24, pp. 5100-5108
[4] Hu, Y., *et al.*, Study of Multiple Steady Solutions for the 2D Natural Convection in a Concentric Horizontal Annulus with a Constant Heat Flux Wall Using Immersed Boundary-Lattice Boltzmann Method, *International Journal of Heat and Mass Transfer*, *81* (2015), Feb., pp. 591-601
[5] Mojtabi, A., Caltagirone, J. P., Analyse du transfert de chaleur en convection mixte laminaire entre deux cylindres coaxiaux horizontaux, *International Journal of Heat and Mass Transfer*, *23* (1980), 10, pp. 1369-137
[6] Mohammed, H. A., *et al.*, Experimental Study of Forced and Free Convective Heat Transfer in the Thermal Entry Region of Horizontal Concentric Annuli, *International Communications in Heat and Mass Transfer*, *37* (2010), 7, pp. 739-747
[7] Kotake, S., Hattori, N., Combined Forced and Free Convection Heat Transfer for Fully-Developed Laminar Flow in Horizontal Annuli, *International Journal of Heat and Mass Transfer*, *28* (1985), 11, pp. 2113-2120
[8] Nazrul, I., *et al.*, Mixed Convection Heat Transfer in the Entrance Region of Horizontal Annuli*, Int. Journal Heat Mass Transfer*, *44* (2001), 11, pp. 2107-2120
[9] Touahri, S., Boufendi, T., Conjugate Heat Transfer with Variable Fluid Properties in a Heated Horizontal Annulus, *Heat Transfer Research*, *64* (2015), 11, pp. 1019-1038
[10] Touahri, S., Boufendi, T., Numerical Study of the Conjugate Heat Transfer in a Horizontal Pipe Heated by Joulean Effect, *Thermal Sciences*, *16* (2012), 1, pp. 53-67
[11] Basant, K. J., *et al.*, Steady Fully Developed Mixed Convection Flow in a Vertical Micro-Concentric-Annulus with Heat Generating/Absorbing Fluid: An Exact Solution, *Ain Shams Engineering Journal*, *9* (2018), 4, pp. 1289-1301
[12] Oni, M. O., Combined Effect of Heat Source, Porosity and Thermal Radiation on Mixed Convection Flow in a Vertical Annulus: An Exact Solution, *Engineering Science and Technology, an International Journal*, *20* (2017), 1, pp. 518-527
[13] Quintino, A., *et al.*, Buoyancy-Induced Convection of Water-Based Nanofluids in Differentially- Heated Horizontal Semi-Annuli, *Thermal Sciences*, *21* (2017), 6A, pp. 2643-2660
[14] Labsi, N., *et al.*, Viscous Dissipation Effect on the Flow of a Thermodependent Hershel-Bulkley Fluid, *Thermal Sciences*, *19* (2015), 5, pp. 1553-1564
[15] Baehr, H. D., Stephan, K., *Heat and Mass Transfer*, Springer-Verlag, Berlin, 1998

[16] Churchill, S. W., Chu, H. S., Correlating Equation for Laminar and Turbulent Free Convection From a Horizontal Cylinder, *International Journal Heat Mass Transfer*, *18* (1975), 9, pp. 1049-1053
[17] Patankar, S. V., *Numerical Heat Transfer and Fluid Flow*, McGraw-Hill, New York, USA, 1980
[18] Carlo, N., Guidice, S. D., Finite Element Analysis of Laminar Mixed Convection in the Entrance Region of Horizontal Annular Ducts, *Numerical Heat Transfer, Part A*, *29* (1996), 3, pp. 313-330

Paper submitted: October 13, 2017
Paper revised: January 9, 2018
Paper accepted: January 30, 2018